Materials Research Proceedings 41 (2024) 110-119 https://doi.org/10.21741/9781644903131-12

Improving the structural integrity of challenging to manufacture LPBF components with toolpath correction

JENSCH Felix[1,a], EISSING Katharina[2,b], WILLIAMS Richard[2,c], TRAUTMAN Marcus[2,d], YANG Yitong[3,e], DUBININ Sergej[1,f], FERGANI Omar[2,g], HÄRTEL Sebastian [1,h]

[1]Chair of Hybrid Manufacturing (FHF), Brandenburg University of Technology, 03046 Cottbus, Germany

[2]1000 Kelvin GmbH, 10625 Berlin, Germany

[3]Chair of Physical Metallurgy and Materials Technology, Brandenburg University of Technology, 03046 Cottbus, Germany

[a]felix.jensch@b-tu.de; [b]katharina.eissing@1000kelvin.com; [c]richard.williams@1000kelvin.com; [d]marcus.trautmann@1000kelvin.com, [e]yang@b-tu.de, [f]dubinser@b-tu.de, [g]omar@1000kelvin.com, [h]haertel@b-tu.de

Keywords: LPBF-Process, Machine Learning, Microstructural Investigation

Abstract. This work deals with the influence of optimised exposure strategies on the distortion and microstructure of components susceptible to overheating and warpage. Therefore, different distortion-prone specimen geometries of 316L were fabricated with the standard parameters, as well as with exposure strategies optimised by machine learning, which were generated using the AMAIZE software package. The manufactured samples were analysed with regard to distortion. The results of the distortion analysis were then linked with the results of the digital tomography from AMAIZE. Furthermore, components were manufactured that tend to overheat due to their geometry and orientation on the substrate plate. The influence of overheating during the LPBF process on the microstructure and porosity was investigated along the build-up direction by means of an EBSD analysis and a porosity analysis. With the presented approach for optimising the exposure strategy with AMAIZE, it could be shown that a successful production of distortion-prone components with a porosity of less than 1 % is possible in the first trial.

Introduction

Due to increasing requirements in terms of lightweight construction, customisation and the performance of components in aerospace, medical technology, the automotive industry and many other sectors, additive manufacturing is becoming increasingly important. This is reflected in the increase in market volume from 3 billion USD in 2013 to almost 12 billion USD in 2019 [1]. The LPBF process has established itself as an important method in metal additive manufacturing, as the low layer thickness and the small focal diameter of the laser, often less than 100 µm, allow components with a complex geometry to be produced close to the final shape. The laser melts the powder locally, which results in a large amount of heat energy being generated during the process, depending on the process parameters [2]. As the surrounding metal powder only dissipates this thermal energy, depending on the particle shape and size, to a limited extent, it is mainly dissipated through the already solidified layers of the component generating large, non-uniform temperature gradients [3, 4]. In order to produce components with large overhang angles, support structures are used in these areas, which on the one hand support heat dissipation, but on the other hand result in higher material consumption, longer production times and time-consuming removal procedures [5, 6]. This limits the advantage of environmentally friendly near-net-shape production and reduces productivity due to the required post-processing to remove the support structures.

Furthermore, component areas that are connected to support structures have a poorer surface quality, which has a negative impact on fatigue strength [7].

Complex geometries also generally have areas of different thicknesses. With a continuous increase in the cross-sectional area from layer to layer, the heat introduced accumulates in the narrow areas. Due to the different temperature history in different areas of the component, a locally varying microstructure and internal stresses develop [8, 9]. Depending on the heat history, martensitic, bainitic, ferritic, pearlitic or austenitic structures can develop in steels [10]. These inhomogeneities in the microstructure cause the mechanical properties of complex components to vary locally [11]. This can only be considered with great effort when designing the components. The production of components with a homogeneous microstructure would therefore increase component reliability and speed up qualification processes in areas such as aviation.

To melt the powder, the laser is guided over the powder layer in meander-shaped paths. However, due to the usually complex geometries of the components, the length of the exposure vectors varies. With constant pause times between adjacent vectors and an unchanged scanning speed, areas with short vectors are exposed faster with the same energy input. Accordingly, the temperature is locally higher in areas with short exposure vectors, which leads to uneven heat distribution in the component [12, 13, 14, 15, 16]. This uneven application of energy leads to an increase in internal stress. If the residual component stresses exceed a certain value, that is defined by the strength of the support structures or the base metal, the component is deformed during the manufacturing process [17]. If the component is severely distorted, the recoater can collide with the component, which leads to the production process being cancelled.

A more even heat distribution in the component can be achieved, for example, through feedback control by means of monitoring and an adjustment of the process parameters based on this. Kavas et. al. have presented a variant in which the laser power is automatically adjusted within a defined range during the process by taking images with a thermographic camera in order to achieve a stable interlayer temperature [18]. In 2023, EOS published the "Smart Fusion" closed-loop control system, which uses optical tomography data to adjust the laser power layer by layer using correction factors with the aim of achieving a homogeneous temperature distribution in the component [19]. The aim of this work is to demonstrate that the AI software AMAIZE from the company 1000 Kelvin can be used to influence the process parameters using machine learning algorithms in such a way that the component distortion can be reduced and the component quality improved. This allows the development of defects to be predicted and avoided even before the process starts.

Materials and Methods

Part Manufacturing

The distortion-prone samples and the cubes were manufactured on an EOS M290 system from EOS GmbH, which has a focus diameter of approx. 0.08 mm and in which an argon atmosphere was set up. Stainless steel alloy 316L powder with a particle size between 20 and 45 µm was used, which was produced by m4p material solutions GmbH. The powder layer was applied using a carbon fibre brush. The process parameters shown in Table 1 were used for all LPBF processes carried out.

Table 1: Process parameters used in the LPBF processes

Processing Parameters	Laser Power	Scanning speed	Hatching distance	Layer thickness
Value	200 W	900 mm/s	0,1 mm	0,04 mm

As a reference, the components were initially manufactured without optimising the exposure strategy with the parameters mentioned (Figure 1 a)). Subsequently, the exposure strategy for the

components of the same build job was optimised with AMAIZE. For example, the pause times between adjacent vectors were adjusted through optimisation in order to achieve uniform heat distribution across the entire component. With these optimisations, the build job was then manufactured again with the process parameters from Table 1 in an argon atmosphere. (Figure 1 b)). A 25 x 25 x 25 mm³ cube was then produced on a rod with a diameter of 2.5 mm, which overheats due to heat dissipation constriction from the cube to the rod (Figure 1). To analyse the porosity and microstructure, the cube was separated by wire EDM as shown in Figure 1 d after removing the rod.

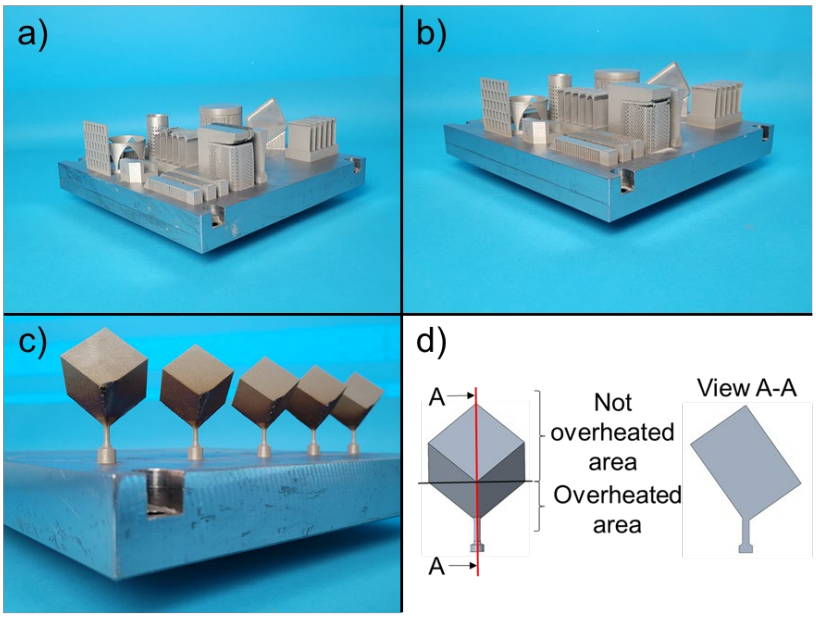

Figure 1: a) distortion-prone samples without optimised exposure strategy; b) distortion-prone specimens with optimised exposure strategy; c) LPBF-manufactured components that tend to overheat; d) cut of the cubes for the porosity analysis and the EBSD analysis

3D-Scanning

The 3D scanning of the components was carried out using the ATOS 5 - 8M digitalisation platform from GOM GmbH. The resolution of the two CMOS cameras is 3357 x 2456 pixels, whereby the measurement was carried out over a measuring field of 500 x 370 mm². The measurement was performed after separating the components from the substrate plate. The scanned geometries were then superimposed with the CAD files of the manufactured components in the GOM Inspect software package from GOM GmbH and the deviations between the two geometries were measured digitally (Figure *2*).

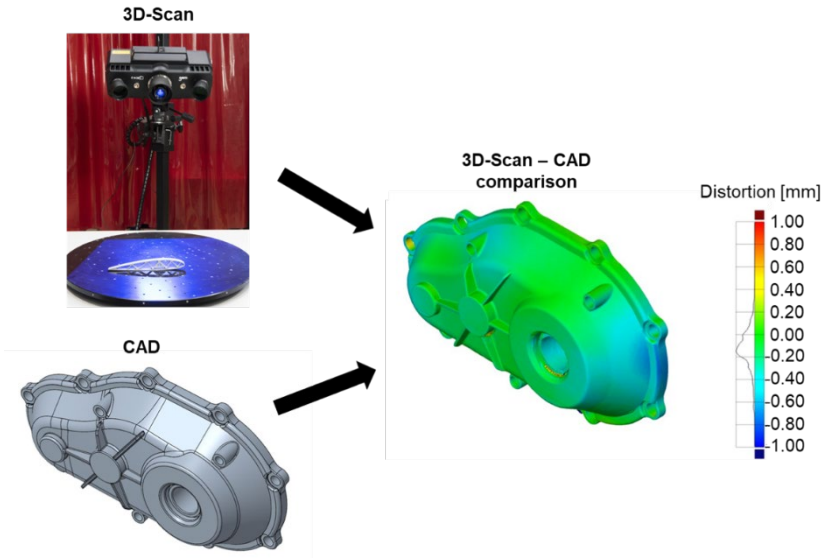

Figure 2: Determination of the distortion with the ATOS 5 - 8M system

Microstructure analysis

For metallographic examination, the cubes were cut along the build-up direction, from the connection to the rod to the tip. The samples were then cold-embedded, ground with 240-4000 grit sandpaper and then polished with 6-3 µm diamond suspension and followed with the 0.15 µm OPS polish. The porosity was analysed using the VHX 7000 digital microscope and software from the KEYENCE DEUTSCHLAND GmbH. The EBSD analysis was performed with the field-free ultra-high-resolution scanning electron microscope TESCAN AMBER from TESCAN GmbH, which is equipped with an energy dispersive X-ray spectrometer and a high-resolution electron backscatter diffraction detector Symmetry S3 EBSD system from Oxford instruments plc. The EBSD data with was recorded with a step size of 2.02 µm and analysed with the AZtecCrystal software from Oxford Instruments plc.

Results and discussion

Distortion of test geometries manufactured with and without AMAIZE

As the optimisation of the process parameters and the exposure strategy with AMAIZE is to be tested for different geometric elements, such as material accumulations or thin walls, components that tend to warp during the LPBF process were manufactured, 3D-scanned and compared to the CAD-file. To show the effect of the adjusted parameters, the components were first manufactured with the standard parameters and then with the optimised parameters. In the angled component, heat builds up at the transition from the component to the support. This is caused by the reduced thermal conductivity of the support structure compared to solid material [20]. Furthermore, the scan vectors are shorter due to the contour boundaries at edges and corners, which, as described by Liu et al., promotes heat accumulation due to the shortened time intervals when exposing adjacent vectors [12]. The resulting overheating causes distortion here. The aim here was to minimize the local heat input at the edges and corners of the component in order to prevent the weakly designed support from tearing off the component. Parameter optimisation with AMAIZE is used to control the pause times of short, adjacent scan vectors in such a way that the heat introduced is dissipated as evenly as possible. Figure 1 a shows that the support is torn off over the entire length of the overhanging component area without optimizing the parameters. When using the optimized process parameters, the support structure essentially tears in the structure itself, which can be avoided by designing the structure more densely. Figure 3 also shows that the warpage does not extend as far into the component with the optimised parameters.

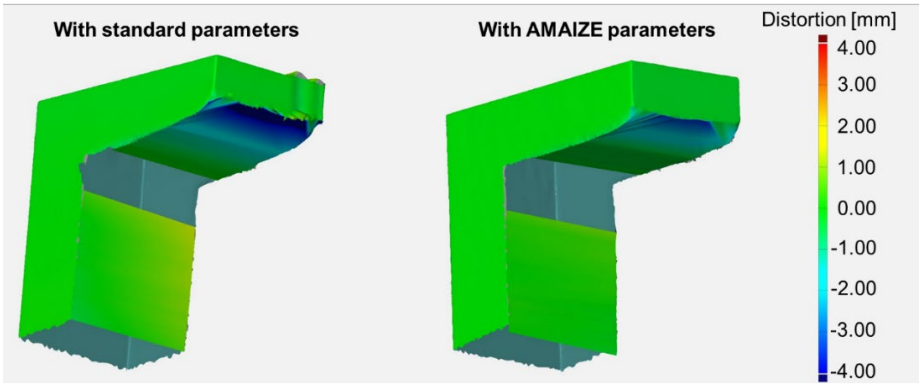

Figure 3: Comparison of the distortion between the manufactured winkle and the CAD file without (left) and with (right) optimisation of the manufacturing parameters

During the production of the thin walls with the accumulation of material on the top, the components warped very strongly when the non-optimised process parameters were used. This damaged the carbon fibre brush used to apply the powder, which also resulted in major geometric deviations in other components of the build job. As a result, one wall of the structure suffered bonding failures and ultimately the complete loss of the connection between the component and the subsequently melted powder material, which also damaged the two walls behind it. This effect was avoided after optimising the exposure strategy with AMAIZE (Figure *4*). The three walls on the left-hand side of the component also exhibit less warpage after optimisation than the walls produced with the standard parameters. Due to the small cross-sectional area of the walls, the thermal energy introduced cannot be completely dissipated. This leads to a heat build-up in the area of the material accumulation at the tip, which is the cause of the warpage. Contrary to expectations, the greatest distortion occurred in the wall with the smallest accumulation of material at the top. One reason for this is that the exposure vectors are shorter for the smaller accumulations of material. As a result, the exposure of neighbouring vectors is faster, which results in higher local heat generation in the short term than with longer exposure vectors, what subsequently causes warping.

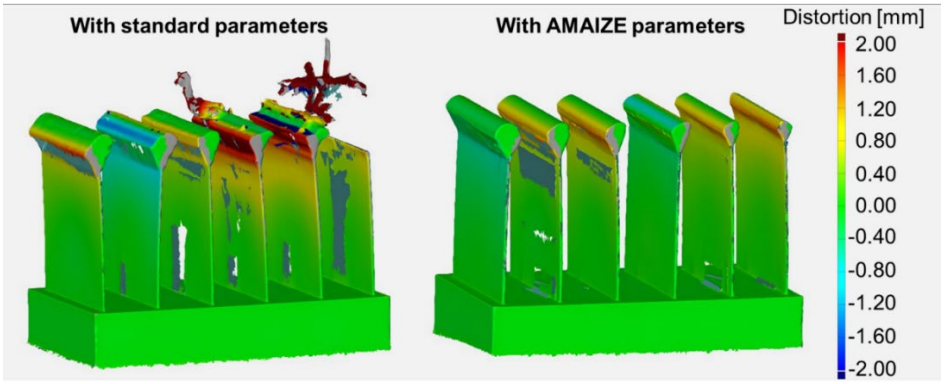

Figure 4: Comparison of the distortion between the manufactured thin walls and the CAD file without (left) and with (right) optimisation of the manufacturing parameters

Linking warping with the AMAIZE digital tomography

For a quick assessment of the thermal energy input, a two- and three-dimensional digital tomography of the components to be manufactured in the LPBF process is created in AMAIZE. Figure 5 shows the results of the digital tomography from various layers located in the warped area shortly after the end of the support structure for the angle. It can be seen that an increased energy input is predicted in layer 1015 over a large area of the exposed surface. This result reflects the

Materials Research Proceedings 41 (2024) 110-119 https://doi.org/10.21741/9781644903131-12

poorer heat dissipation through the support structure and reflects the distortion in this area. After optimising the exposure parameters, the predicted heat development in this area is significantly lower. An increased temperature is detected at regular intervals in the other layers. This is due to the strip-like exposure strategy used to produce the components and the meandering exposure of the individual exposure vectors within these strips. After the exposure of a vector at the end of the strip has been completed, the adjacent vector starts, usually without waiting time, at a definable distance, which is often only between 50 and 200 µm. This results in a higher energy input for a short time in this area than in the centre of the strips. The machine learning algorithm in AMAIZE influences the pause times between adjacent vectors based on the thermophysical properties, which are based on the geometry and the other process parameters. This significantly reduces overheating at the ends of the strips.

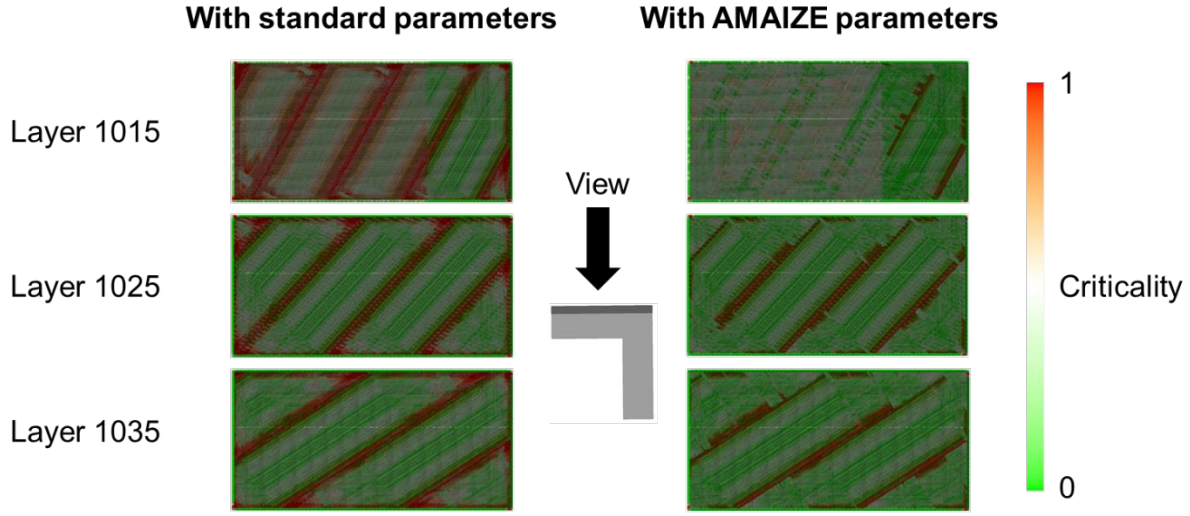

Figure 5: Digital tomography on different layers of the winkle component

As with the angle element, the heat development in the thin walls is greater with the standard parameters than with the parameters optimised by AMAIZE. Figure 6 shows three of the layers where the accumulation of material on the wall begins. It is notable that the walls with the smaller accumulations of material are predicted to have particularly high heat generation with the standard parameters. This reflects the distortion in these areas from the LPBF-test. One possible cause, as already suspected, is the short length of the scan vectors in this area, with the cross-section increasing from layer to layer. The resulting high heat input cannot be dissipated sufficiently through the wall, which is why distortion occurs. After optimising the parameters using AMAIZE, a reduction in heat development is achieved for these walls in particular, which is again due to the increased pause times between adjacent exposure vectors.

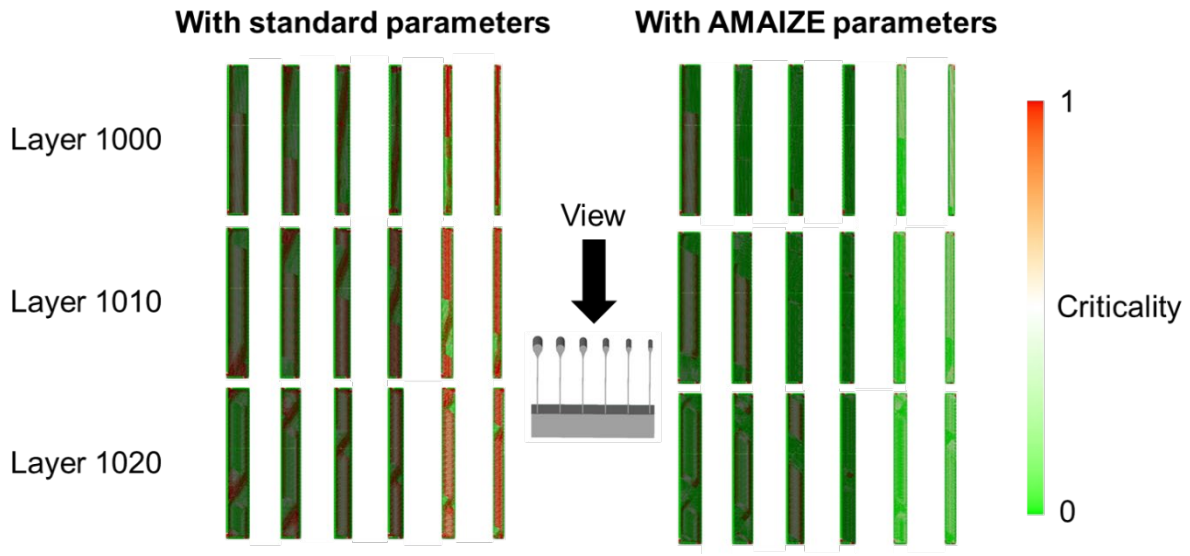

Figure 6: Digital tomography on different layers of the thin wall component

Influence of overheating on the porosity and the microstructure

The cubes on a rod have been successfully produced using AMAIZE optimized exposure strategy. We differentiate between the top and bottom sections of the cube due to observable variations. Specifically, the bottom part exhibits signs of overheating, such as external oxidation, indicating a distinct thermal signature compared to the top section.

To evaluate the cubes produced in Figure 1 c/d, the cubes were examined for their porosity and microstructure in the bottom region, which shows tarnishing on the surface, and the upper top area. The porosity is very low at 0.04 % in the bottom area and 0.02 % in the top area over the entire sample (Figure *7*). It is assumed that due to the uniform overheating over the entire surface, the thermal gradient between the exposed area and the surrounding areas was lower, so that the melt pool flows were lower than for strongly cooled surfaces, in accordance with the Marangoni effect [21]. Figure *7* b shows an increased number of pores between 5 and 15 µm in the overheated and non-overheated areas. It is notable that the overheated area sometimes has very large pores of over 100 µm. One reason for this may be a greater melt pool depth due to the already high surface temperature, which has led to the formation of larger pores corresponding to the keyhole effect [22].

Using an EBSD analysis, an average grain size of approx. 91 µm was determined in the overheated area. In the non-overheated upper area of the cube, the average grain size of approx. 48 µm was only about half of this. As the overheating in the lower area of the cube is effective for almost the entire duration of the printing process, effects similar to those of heat treatment already occur here. The increased temperature results in greater grain growth, which leads to lower tensile strength and higher elongation at break [23]. Figure *7* c and d also show that the grains are stretched along the direction in which they are built up. This results from the temperature gradient, which is caused by the dissipation of the heat introduced in the negative build-up direction. As the heat accumulated in the overheated area, the grains could also grow at right angles to the build-up direction, although this effect was less pronounced than expected.

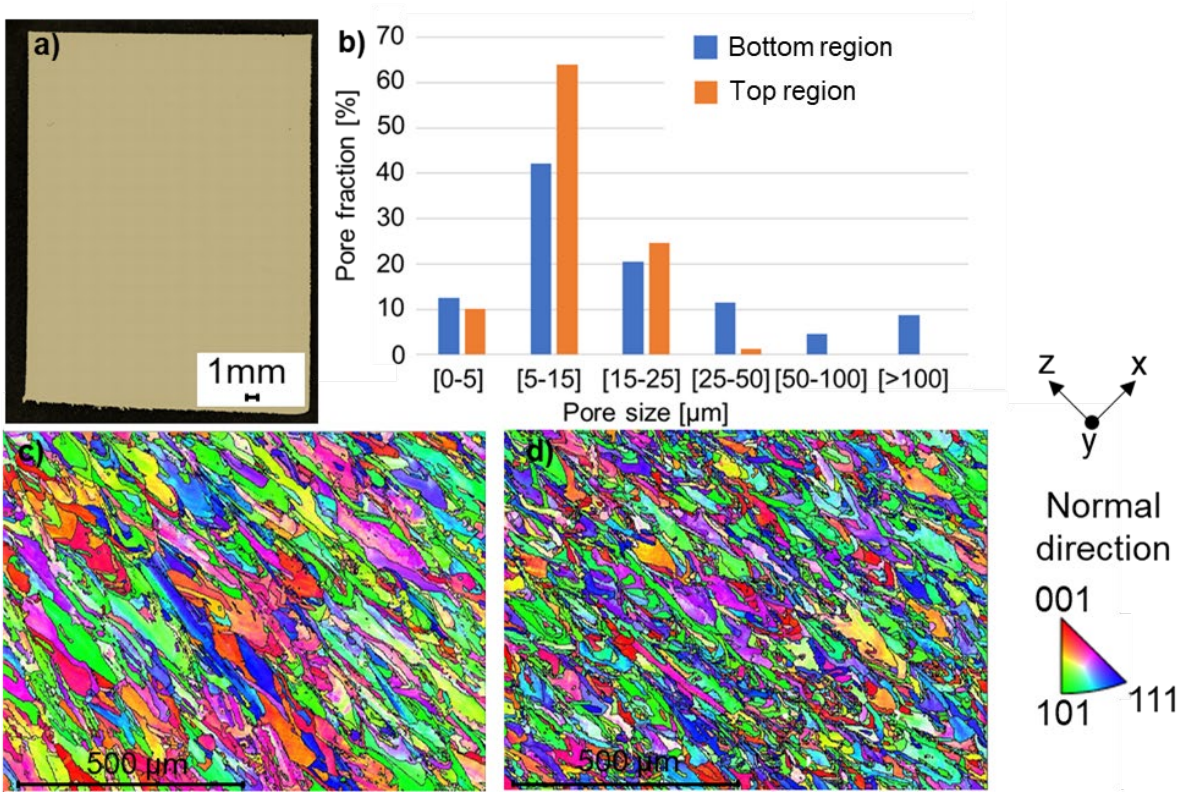

Figure 7: overview of the a) porosity and b) the pore distribution as well as an EBSD overview of c) an overheated area and d) a not overheated area

Conclusions and outlook

In this work, various components susceptible to distortion were manufactured from 316L with standard parameters and with parameters optimised by a machine learning algorithm and investigated with regard to distortion. Furthermore, geometries that are prone to severe overheating were analysed in terms of porosity and microstructure. Based on the results, the following conclusions can be drawn:

- Components that are difficult to manufacture in the LPBF process were successfully produced in the first attempt after optimizing the exposure strategy with AMAIZE
- By utilizing advanced machine learning algorithms to adjust the exposure strategy and process parameters, we can achieve a more uniform distribution of the laser's energy throughout the component. This enhanced control helps in evenly heating the material, thereby significantly reducing the likelihood of distortion during the manufacturing process.
- Regardless of the overheating of the component, the porosity remained roughly identical in all areas of the component, whereby the size of the pores is larger in overheated areas
- As the high temperatures in overheated areas are maintained over the duration of the process, this results in increased grain growth, which leads to an inhomogeneous microstructure and therefore varying mechanical properties in the component

By optimising the process parameters with machine learning algorithms, a more homogeneous microstructure and therefore better mechanical properties can be achieved due to a more even heat distribution in the component. This demonstrates a pathway to reduce build failures in metal AM, improving the economic viability and reducing the environmental footprint of the process. Further, such toolpath corrections can enable process engineers to use fewer support structures, increasing

freedom to designers and reducing the cost per part. The machine learning algorithm is to be trained further as part of further investigations. For this purpose, monitoring data will also be recorded using a thermographic camera, melt pool monitoring or optical tomography, which will map the temperature history of the component and thus check and improve the accuracy of the algorithm. The aim is to produce components with a homogeneous microstructure and therefore homogeneous mechanical properties.

Reference

[1] C. Tan, F. Weng, S. Sui, Y. Chew und G. Bi, „Progress and perspectives in laser additive manufacturing of key aeroengine materials," *International Journal of Machine Tools and Manufacture,* 2021. https://doi.org/10.1016/j.ijmachtools.2021.103804

[2] W. Di, Y. Yongqiang, S. Xubin und C. Yonghua, „Study on energy input and its influences on single-track, multi-track, and multi-layer in SLM," *International Journal of Advanced Manufacturing Technology,* 2012. https://doi.org/10.1007/s00170-011-3443-y

[3] J. Gan, Z. Zhou und A. Yu, „Effect of particle shape and size on effective thermal conductivity of packed beds," *Powder Technology,* 2017. https://doi.org/10.1016/j.powtec.2017.01.024

[4] L. C. Wei, L. E. Ehrlich, M. J. Powell-Palm, C. Montgomery, J. Beuth und J. A. Malen, „Thermal conductivity of metal powders for powder bed additive manufacturing," *Additive Manufacturing,* 2018. https://doi.org/10.1016/j.addma.2018.02.002

[5] T. Miki und S. Nishiwaki, „Topology optimization of the support structure for heat dissipation in additive manufacturing," *Finite Elements in Analysis & Design,* 2022. https://doi.org/10.1016/j.finel.2021.103708

[6] S. C. Subedi, A. Shahba, M. Thevamaran, D. J. Thoma und K. Suresh, „Towards the optimal design of support structures for laser powder bed fusion-based metal additive manufacturing via thermal equivalent static loads," *Additive Manufacturing,* 2022. https://doi.org/10.1016/j.addma.2022.102956

[7] J. Elambasseril, J. Rogers, C. Wallbrink, D. Munk, M. Leary und M. Qian, „Laser powder bed fusion additive manufacturing (LPBF-AM): the influence of design features and LPBF variables on surface topography and effect on fatigue properties," *Critical Reviews in Solid State and Materials Sciences,* 2023. https://doi.org/10.1080/10408436.2022.2041396

[8] G. Mohr, N. Scheuschner und K. Hilgenberg, „In situ heat accumulation by geometrical features obstructing heat flux and by reduced inter layer times in laser powder bed fusion of AISI 316L stainless steel," *Procedia CIRP,* 2020. https://doi.org/10.1016/j.procir.2020.09.030

[9] J. Munk, E. Breitbarth, T. Siemer, N. Pirch und C. Häfner, „Geometry Effect on Microstructure and Mechanical Properties in Laser Powder Bed Fusion of Ti-6Al-4V," *metals,* 2022. https://doi.org/10.3390/met12030482

[10] S. Astafurov und E. Astafurova, „Phase Composition of Austenitic Stainless Steels in Additive Manufacturing: A Review," *Metals,* 2021. https://doi.org/10.3390/met11071052

[11] T. A. Rodrigues, V. Duarte, J. A. Avila, T. G. Santos, R. Miranda und J. Oliveira, „Wire and arc additive manufacturing of HSLA steel: Effect of thermal cycles on microstructure and mechanical properties," *Additive Manufacturing,* 2019. https://doi.org/10.1016/j.addma.2019.03.029

[12] Y. Liu, J. Li, K. Xu, T. Cheng, D. Zhao, W. Li, Q. Teng und Q. Wei, „An optimized scanning strategy to mitigate excessive heat accumulation caused by short scanning lines in laser

powder bed fusion process," *Additive Manufacturing,* 2022. https://doi.org/10.1016/j.addma.2022.103256

[13] L. Wang, X. Jiang, Y. Zhu, X. Zhu, J. Sun und B. Yan, „An approach to predict the residual stress and distortion during the selective laser melting of AlSi10Mg parts," *The International Journal of Advanced Manufacturing Technology,* 2018. https://doi.org/10.1007/s00170-018-2207-3

[14] D. Dai, D. Gu, Q. Ge, Y. Li, X. Shi, Y. Sun und S. Li, „Mesoscopic study of thermal behavior, fluid dynamics and surface morphology during selective laser melting of Ti-based composites," *Computational Materials Science,* 2020. https://doi.org/10.1016/j.commatsci.2020.109598

[15] Z. Li, R. Xu, Z. Zhang und I. Kucukkoc, „The influence of scan length on fabricating thin-walled components in selective laser melting," *International Journal of Machine Tools and Manufacture,* 2018. https://doi.org/10.1016/j.ijmachtools.2017.11.012

[16] Y.-L. Lo, B.-Y. Liu und H.-C. Tran, „Optimized hatch space selection in double-scanning track selective laser melting process," *The International Journal of Advanced Manufacturing Technology,* 2019.

[17] N. Levkulich, S. Semiatin, J. Gockel, J. Middendorf, A. DeWald und N. Klingbeil, „The effect of process parameters on residual stress evolution and distortion in the laser powder bed fusion of Ti-6Al-4V," *Additive Manufacturing,* 2019. https://doi.org/10.1016/j.addma.2019.05.015

[18] B. Kavas, E. C. Balta, M. Tucker, A. Rupenyan, J. Lygeros und M. Bambach, „Layer-to-layer closed-loop feedback control application for inter-layer temperature stabilization in laser powder bed fusion," *Additive Manufacturing,* 2023. https://doi.org/10.2139/ssrn.4496744

[19] A. Yağmur, I. Pääkkönen und A. Miles, „The Hitchhiker's Guide to Smart Fusion," July 2023. [Online]. Available: https://www.eos.info/smart-fusion.

[20] L. White, X. Liang, G. Zhang, J. Cagan und Y. J. Zhang, „Coupling Simulated Annealing and Homogenization to Design Thermally Conductive Hybrid Lattice Support Structures for LPBF," *Proceedings of the ASME 2023,* 2023. https://doi.org/10.1115/DETC2023-114953

[21] M. Rombouts, J. Kruth, L. Froyen und P. Mercelis, „Fundamentals of Selective Laser Melting of alloyed steel powders," *CIRP Annals,* 2006. https://doi.org/10.1016/S0007-8506(07)60395-3

[22] G. Kasperovich, J. Haubrich, J. Gussone und G. Requena, „Correlation between porosity and processing parameters in TiAl6V4 produced by selective laser melting," *Materials and Design,* 2016. https://doi.org/10.1016/j.matdes.2016.05.070

[23] A. Yadollahi, N. Shansaei, S. M. Thompson und D. W. Seely, „Effects of process time interval and heat treatment on the mechanical and microstructural properties of direct laser deposited 316L stainless steel," *Materials Science & Engineering A,* 2015. https://doi.org/10.1016/j.msea.2015.07.056